# Statistics-based Numerical Study on the Influential Area of Basin Effects for Shallow Basins

**C. Zhu[1], D. Thambiratnam[2], J. Zhang[3] and C. Gallage[4]**

1. Corresponding Author. PhD Candidate, School of Civil Engineering and the Built Environment, Queensland University of Technology, Australia.
   Email: c2.zhu@qut.edu.au

2. Professor, School of Civil Engineering and the Built Environment, Queensland University of Technology, Australia.
   Email: d.thambiratnam@qut.edu.au

3. Professor, School of Civil Engineering, Southwest Jiaotong University, China.
   Email: jianzhang1102@home.swjtu.edu.cn

4. Senior Lecturer, School of Civil Engineering and the Built Environment, Queensland University of Technology, Australia.
   Email: chaminda.gallage@qut.edu.au

## Abstract

Basin effects have been proven to be of significance to seismic ground motion by many researchers, yet 1D site response analysis, especially based on equivalent nonlinear method, has been dominating in engineering practice. With the aim of contributing to the incorporation of complex site effects into seismic provisions, quantification of the influential area of basin effects for shallow basins is conducted in this research based on statistics-based numerical analysis to a total of 50 vertically heterogeneous basin configurations subject to real earthquakes recorded on rock sites. It is concluded that for a shallow basin, calibration to the acceleration spectra is only needed to locations within the close-to-edge region of which the width is linear correlated to the basin depth.

**Keywords**: site effects, basin, 2D, surface waves, statistics

## 1. Introduction

Researchers have observed and then recognised the basin effects as the topographical, geotechnical and geophysical effect of superficial soil layers on strong ground motion (Hanks, 1975; Tucker and King, 1984; King and Tucker, 1984; Bard and Bouchon, 1980a,b) for several decades. Basin effects have received much attention as they not only involve spatially varying and elongated ground motion as well as anomalous amplification, but also because of the fact that many urban areas in the world, such as Los Angeles, Tokyo, Osaka and Kathmandu, are situated atop alluvial basin configurations.

Numerous studies on basin effects have thus been conducted (Aki and Larner, 1970; Trifunac, 1971; Bard and Bouchon, 1980a, b; among others). These studies contribute to the understanding of the underpinning mechanisms and the features exclusive to multidimensional basin effects, including (a) 2D resonance (Bard and Bouchon, 1985; Rail and Ling, 1992; Roten et al., 2006; Ermert et al., 2014, among many others); (b) Surface waves (Bard and Bouchon, 1980a, b; Raptakis, et al., 2004; Makra et al., 2016; Zhu et al., 2015, 2016; Zhu and Thambiratnam, 2016, among many others); (c) Other wave phenomena due to the multidimensional geometries, such as focusing effect (Hudson, 1963, among many others).

Although the mechanism of the multi-dimensional site effects have long been clarified, modern seismic regulations are still mainly based on 1D assumptions which has proved to be unable to reproduce the ground motions of some basins where basin effects need to be taken into account (Chávez-García and Faccioli, 2000; Makra and Chávez-García, 2016). To contribute to the eventual incorporation of the multi-dimensional site effects into seismic codes, a quantitative estimation to the influential area of basin effects is necessary. Given the uncertain nature of this problem, a statistical study is needed to provide a compelling result. Therefore, a statistics-based quantitative study on the influential area of basin effects is carried out in this research.

## 2. Methodology

In order to quantify basin effects, some researchers tried to introduce basin depth into ground motion attenuation model through the analysis of strong ground motion data (Trifunac and Lee, 1978, Campbell, 1997; Field, 2000; Lee and Anderson, 2000; Somerville, 2004; Hruby and Bersnev, 2003; Choi et al., 2005, among many others).

Chávez-García and Faccioli (2000) explored a different way by introducing an "aggravation factor" (*AG*) which is defined as the ratio between response spectra computed at the surface of the 2D model and the response spectra computed at the surface of the equivalent 1D model to quantify the additional amplification or de-amplification caused by basin effects, thus bridging the gap between 1D and multi-dimensions (Faccioli and Vanini, 2003; Raptakis et al., 2004; Makra et al., 2005; Vessi and Russo, 2013; Riga, 2015).

Based on the aggravation factor proposed by Chávez-García and Faccioli (2000), a more comprehensive gauge - Spectral Aggravation factor (*SAG*), was introduced in our previous studies (Zhu and Thambiratnam, 2016) to account for both the frequency and spatiality dependency of *AG*:

$$SAG(T/T_0,\ x/L) = \frac{SA_{2D}(T/T_0,\ x/L)}{SA_{1D}(T/T_0,\ x/L)} \tag{1}$$

where $SA_{2D}(T/T_0, x/L)$ and $SA_{1D}(T/T_0, x/L)$ - spectral acceleration (*SA*) at receiver $x/L$ of 2D model and its corresponding 1D model respectively, *x*- distance of a surface point from the basin centre; *L*- basin half-width; *T*- spectral period, $T_0$- fundamental period of the equivalent plane layers of a basin by weighted average method. The present research aims to provide a statistical value of *SAG*.

## 3. Numerical modelling

There exist only a very few basins or valleys to which both detailed information on geometry as well as dynamic property and high-quality strong ground motions are available, which renders it significantly difficult, if not impossible, to conduct statistical study on strong ground motions recorded on a large enough number of real basins. Thus, numerical study on a large number of hypothetic basins is implemented in this study.

### 3.1 Modelling method

Seismic response of a basin is simulated by an explicit FD (finite difference) code- 2DFD_DVS developed by Moczo et al. (2004). This FD method solves the equations of motion in the 2D heterogeneous isotropic viscoelastic structures with a planar free surface. The scheme is 4th-order accurate in space and 2nd-order accurate in time. The computational region is an area of a rectangle with the bottom, left and right sides representing non-reflecting boundaries. Upper cut-off frequency $f_{cut}$ is set to 10 Hz, and correspondingly, the spatial step is one tenth of the minimum wavelength to balance the numerical efficiency and accuracy.

The critical time step of the dynamic analysis is set to satisfy the stability condition for the 4$^{th}$-order staggered grid FD scheme based on the spatial step and maximum *P*-wave velocity of the model:

$$\Delta t \leq \frac{6h}{7\sqrt{2}v_p} \tag{2}$$

where h is the grid spacing, and $v_p$ is the compressional wave velocity.

The rheology of the medium corresponds to the generalised Maxwell body, which makes it possible to guarantee the quality factor ($Q$) variable for different materials but constant within the frequency range of interest. Quality factor for shear ($Q_s$) and compressional ($Q_p$) waves are defined as:

$$Q_s = v_s/10 \tag{3}$$

$$Q_p = 2Q_s \tag{4}$$

where $Q_s$ and $Q_p$ - quality factor for shear and compressional waves respectively; $vs$ - shear wave velocity. This technique was thoroughly verified in details by Makra et al. (2012) and Riga (2015).

## 3.2 Basin configurations

Previous researches show that seismic ground motion of shallow basins is dominated by the propagation of surface waves initiated at basin edges, triggering intense ground motion in the close-to-edge areas, while for deep basins, 2D resonance will be dominant, mobilising the whole basin (Bard and Bouchon, 1985). Since shallow basins present a different ground motion pattern from deep basins when subjected to seismic motion, only shallow basins are studied in the present research.

Based on a preliminary study on several real basin geometries, a generic shallow basin configuration (Fig. 1) is proposed, a symmetrical trapezoidal shape with constant basin half-width $L$=2500 m, to guarantee that all the basins are broad enough so as to eliminate the possibility of 2D resonance (Bard and Bouchon, 1985) without compromising the generality of the basin geometry from an engineering practice perspective.

Our previous study (Zhu, et al., 2016) detailed that, in comparison with 1D analysis, lower peak ground acceleration (*PGA*) and *PGA* shifts above the wedge in 2D analysis arose in essence out of the wave energy loss upon entry into the wedge and the wave deflection by the edge after entry, which was referred to as "wedge effect". The wedge effect is mainly limited to the edge region, of which the aggravation factor is either approximately equal to unity (small dip angle) or less then unity (large dip angle). Due to the slope angel's already-know effects in both qualitative and quantitative senses, $\alpha$ is thus fixed at $45^0$ in the present study.

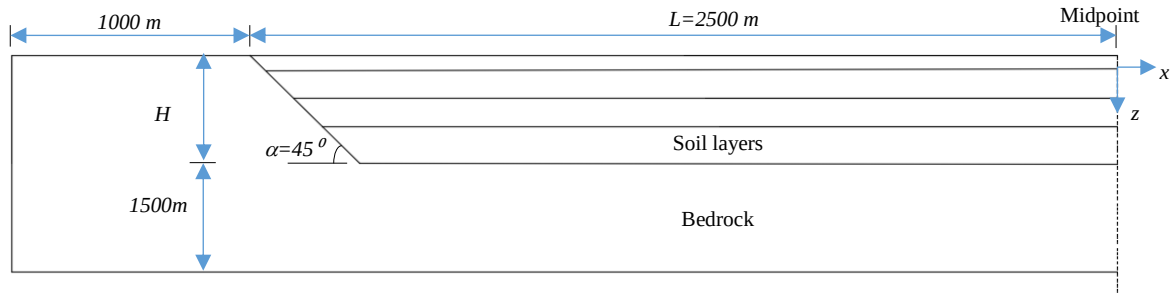


**Fig. 1** Schematic diagram of FD model (only half of the model is displayed because of symmetry)

A total of 50 hypothetic shallow basins with constant $L$ and $\alpha$ (Table 1 in Appendix) are configured with vertical inhomogeneity. Among them, 31 basin models are configured based on real 1D soil profiles (Table 2) compiled from KiK-net database. Another 19 2D configurations are constructed based on hypothetic 1D profile in order to achieve a set of basins well distributed in the $H_{800}$-$v_{s,30}$ chart, as shown in Fig. 2. In Fig. 2, $\boldsymbol{H_{800}}$ presents the depth of the top of the first layer with shear wave velocity greater than 800 m/s and $\boldsymbol{v_{s,30}}$ is the average shear wave velocity of the topmost soil layers within 30m.

The lateral boundaries of the FD model are placed 1000m away from the corresponding basin edges, while the horizontal boundary is set 1500m below the bottom of the basin (Fig. 1), to minimise the influence of any possible boundary reflections. Receivers are evenly distributed along the basin surface with an interval of 20 m.

## 3.3 Input motions

A total of nine strong ground motions (Table 3) recorded on bedrock site ($v_{s,30}$ >760 m/s) are selected from the *Pacific Earthquake Engineering Research Centre Strong Ground Motion Database* as

vertically incident *SH* waves. All these seismic records are baseline-corrected and bandpass-filtered with cut-off frequencies of 0.2 and 10.0 Hz. The acceleration response spectra of these input motions are depicted in Fig. 3, which shows that these excitations are compatible with the spectra recommended for rock site in *Eurocode 8* (**reference spectra**). Each basin models are excited by these nine records. *SAG (T, x/L)* is then averaged over the nine incidences, and the average *SAG (T/T₀, x/L)* is referred to as $\overline{SAG}$ *(T/T₀, x/L)*:

$$\overline{SAG}\,(T/T_0,\ x/L) = \frac{\sum_{i=1}^{9} SAG(T/T_0,\ x/L)}{9} \tag{5}$$

where $\overline{SAG}$ *(T/T₀, x/L)* is the mean of the *SAG*s of the nine excitations.

**Table 2** Soil profile of OSMH01 from KiK-net

| | Thickness (m) | Depth (m) | $v_p$ (m/s) | $v_s$ (m/s) |
|---|---|---|---|---|
| 1 | 6 | 6 | 430 | 180 |
| 2 | 10 | 16 | 1570 | 180 |
| 3 | 14 | 30 | 2430 | 380 |
| 4 | 16 | 46 | 1750 | 280 |
| 5 | 74 | 120 | 1750 | 580 |
| Bedrock | ----- | ----- | 2070 | 900 |

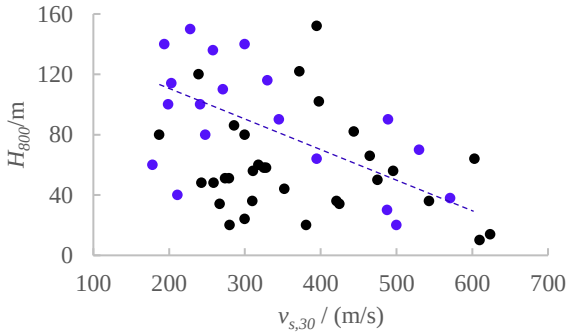


**Fig. 2** $H_{800}$ vs. $v_{s,30}$ at the centre ($x/L$=0) of all basins. $H_{800}$ is the depth to the top of the first layer with shear wave velocity greater than 800 m/s, and $v_{s,30}$ is the average shear wave velocity of the topmost soil layers within 30m. Blue dots are basins configured from hypothetic 1D profile; Black dots are basins configured on real 1D profile from KiK-net;

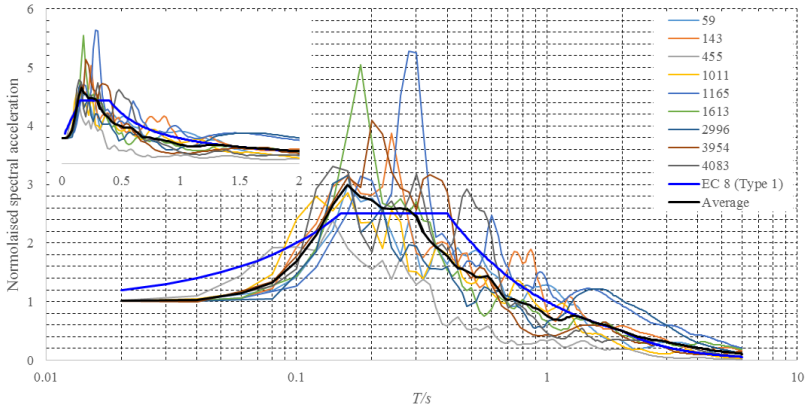


**Fig. 3** Acceleration response spectra (ξ=5%) of the nine input motions in both logarithmic coordinates and Cartesian coordinates (upper left corner).

**Table 3** List of earthquake records used as vertically incident *SH* waves

| Code | Earthquake | Year | Station Name | Magn. | Rrup. (km) | $v_{s,30}$ (m/s) |
|---|---|---|---|---|---|---|
| 59 | "San Fernando" | 1971 | "Cedar Springs Allen Ranch" | 6.6 | 89.72 | 813.48 |
| 143 | "Tabas Iran" | 1978 | "Tabas" | 7.4 | 2.05 | 766.77 |
| 455 | "Morgan Hill" | 1984 | "Gilroy Array #1" | 6.2 | 14.91 | 1428.14 |
| 1011 | "Northridge-01" | 1994 | "LA - Wonderland Ave" | 6.7 | 20.29 | 1222.52 |
| 1165 | "Kocaeli Turkey" | 1999 | "Izmit" | 7.5 | 7.21 | 811.00 |
| 1613 | "Duzce Turkey" | 1999 | "Lamont 1060" | 7.1 | 25.88 | 782.00 |
| 2996 | "Chi-Chi Taiwan-05" | 1999 | "HWA003" | 6.2 | 50.44 | 1525.85 |
| 3954 | "Tottori Japan" | 2000 | "SMNH10" | 6.6 | 15.59 | 967.27 |
| 4083 | "Parkfield-02 CA" | 2004 | "PARKFIELD - TURKEY FLAT #1 (0M)" | 6.0 | 5.29 | 906.96 |

## 4. Results and statistical analysis

Each of these 50 basin models (Table 1) are excited by the nine seismic records (Table 3) for both 1D and 2D scenarios. Thus, a total of 900 cases are simulated in this investigation. $\overline{SAG}$ *(T/T₀, x/L)s* are then derived for each of these 50 basin configurations.

### 4.1 $\overline{SAG}$ *(T/T0, x/L)*

$\overline{SAG}$ *(T/T₀, x/L)s* of basin YMTH10 and FKIH04 are displayed in Fig. 4, which well exemplifies the multivariate nature of $\overline{SAG}$ *(T/T₀, x/L)*, namely *T/T₀- x/l* dependence. It would be too onerous to be applicable if aggravation factor is variable with either different periods or locations. A more applicable indicator than $\overline{SAG}$ *(T/T₀, x/L)* is thus to be explored.

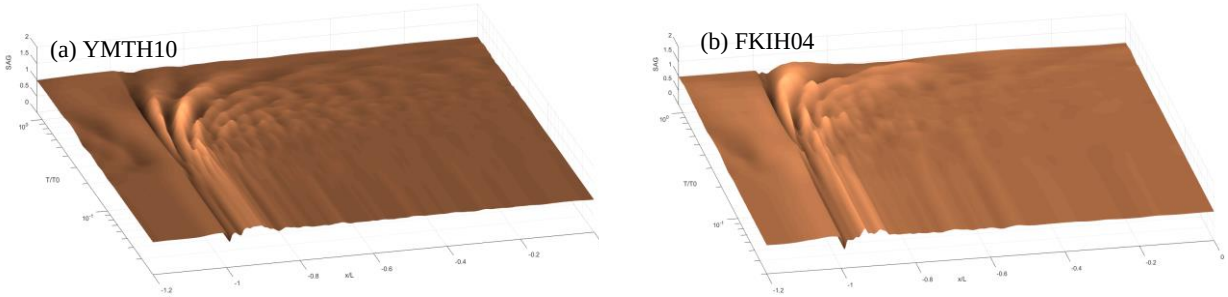


**Fig. 4** $\overline{SAG}$ *(T/T₀, x/L)* of (a) YMTH10 (Type B); and (b) FKIH04 (Type C)

### 4.2 $\overline{SAG}$ *(x/L)*

Fig. 4 is re-presented in a 2D chart as shown in Fig. 5. It can be observed from Fig. 5 that the 2D effect manifests itself only within a certain period range, regardless of location (*x/L*). The same pattern can also be observed from all the other basin configurations. Moreover, this observation is consistent with these of Chávez-García and Faccioli (2000) and Riga (2015) who recommended to consider basin effects within $T \leq T_0$. From the results of this study (Fig. 4 and 5), this period interval is proposed to be from 0.1s to $T_0$. Accordingly, a new indicator is introduced - $\overline{SAG}$ *(x/L)*, which is the maximum value of $\overline{SAG}$ *(T/T₀, x/L)* within $0.1s < T \leq T_0$:

$$\overline{SAG}\,(x/L) = \max\left[\overline{SAG}\,(0.1 < T \leq T_0,\ x/L)\right] \tag{6}$$

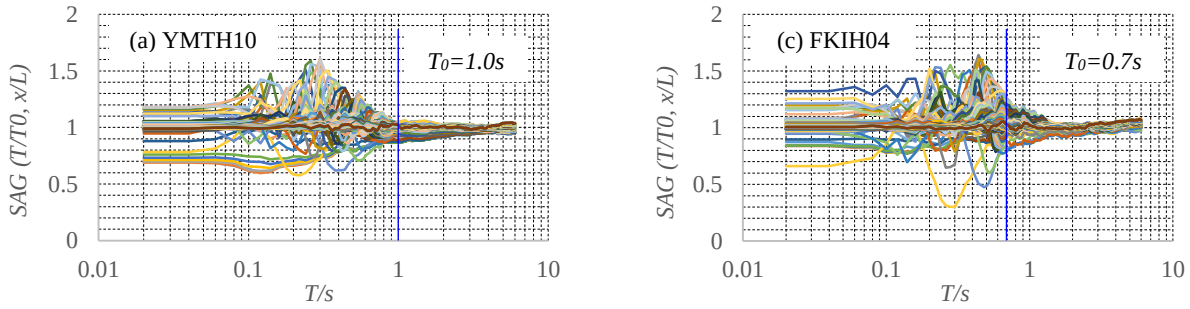


**Fig. 5** $\overline{SAG}$ *(T/T₀, x/L)* of (a) YMTH10 (Type B); and (b) FKIH04 (Type C)

$\overline{SAG}$ *(x/L)s* of model YMTH10 and FKIH04 are depicted in Fig. 6, with a schematic basin configuration presented below. Fig. 6 shows the spatial-dependence of the $\overline{SAG}$ *(x/L)*, which indicates that the 2D site effects influence different basin surface regions to different extents. The fact that the $\overline{SAG}$ *(x/L)* peaks in an area close to basin edge suggests that the implication of 2D effects is only limited to the close-to-edge region, and this is expected for shallow basins (Zhu and Thambiratnam, 2016).

$\overline{SAG}$ *(x/L)s* of all the Type B and C sites are shown in Fig. 7 (a) and (b) respectively, which illustrate the concentration of 2D effects. The maximum values of each $\overline{SAG}$ *(x/L)* curves shown in Fig. 7 (a) and (b) are depicted against $v_{s,30}$ and $H_{800}$ in Fig. 8 (a) and (b) respectively.

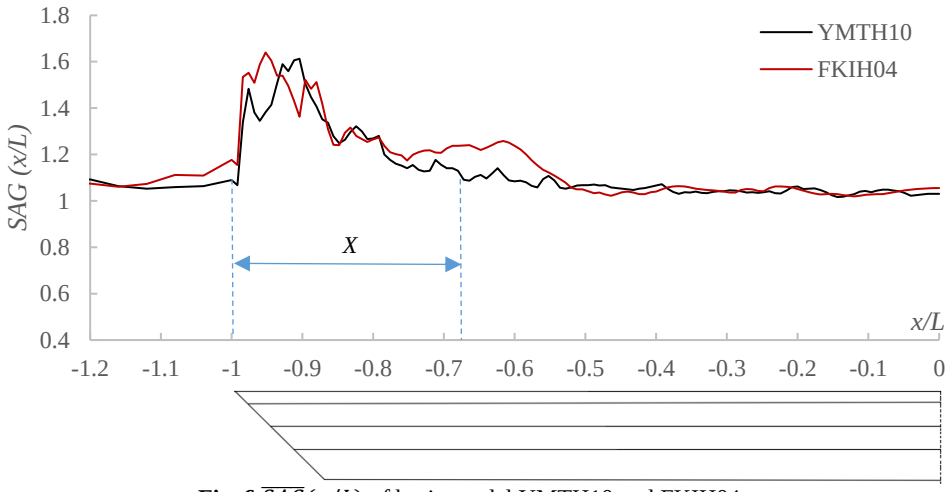


**Fig. 6** $\overline{SAG}(x/L)$ of basin model YMTH10 and FKIH04

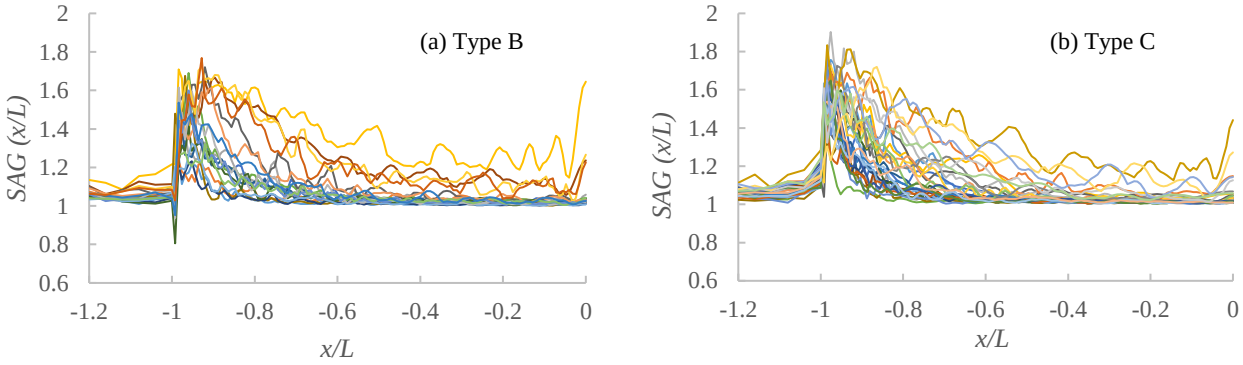


**Fig. 7** $\overline{SAG}(x/L)$ of all (a) Type B basins; and (b) Type C basins

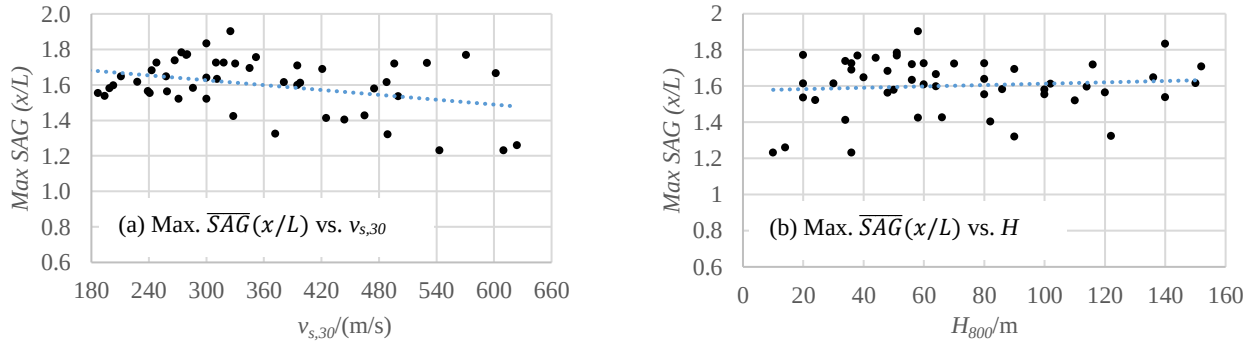


**Fig. 8** Maximum of $\overline{SAG}(x/L)$. (a) Max. $\overline{SAG}(x/L)$ vs. $v_{s,30}$; (b) Max. $\overline{SAG}(x/L)$ vs. $H_{800}$.

In comparison with Type C sites, a broader region of the Type B sites tend to be affected by 2D site effects (Fig. 7), which can be attributed to the generally higher attenuation of Type C sites than Type B sites. However, Type C sites tend to be of higher amplitude than C sites (Fig. 8a), which is in accordance with the conclusion that aggravation factor increases with the impedance ratio (Chávez-García and Faccioli, 2000; Riga, 2015). Fig. 8 also suggests that the maximum values of $\overline{SAG}$ *(x/L)* are less irrelevant to the $H_{800}$ than to $v_{s,30}$.

## 4.3 Influential area

As shown in Fig. 7, 2D site effects cannot extend to the whole surface area of a broad shallow basin, but are limited to an area close to the edges. It is thus imperative to pinpoint the width of this close-to-edge region *X* (Fig. 6). This close-to-edge region is referred to as "influential area" hereafter. The width *X* of the influential area is defined in this study as the distance from the edge ($x_1/L$=-1) to the point $x_2$ whose $\overline{SAG}(x_2/L)$ satisfies the following condition:

$$\overline{SAG}(x_2/L) = \text{Max.}\ \overline{SAG}(x/L) - [\text{Max.}\ \overline{SAG}(x/L) - \text{Min.}\overline{SAG}(x/L)\ ].85\%$$

The widths $X$ of the influential areas of these 50 basin configurations are derived from the $\overline{SAG}$ *(x/L)* (Fig. 7). And then the variations of $X$ versus $v_{s,30}$ and $H_{800}$ are illustrated in Fig. 9 (a) and (b) respectively. Fig. 9 indicates that the width of the influential area $X$ is more correlative to $H$ ($v_s$=800 m/s) than to $v_{s,30}$. A linear fit can be derived from Fig. 9 (b):

$$X = 5H_{800} + 200 \tag{7}$$

where $X$ is the width of the influential area.

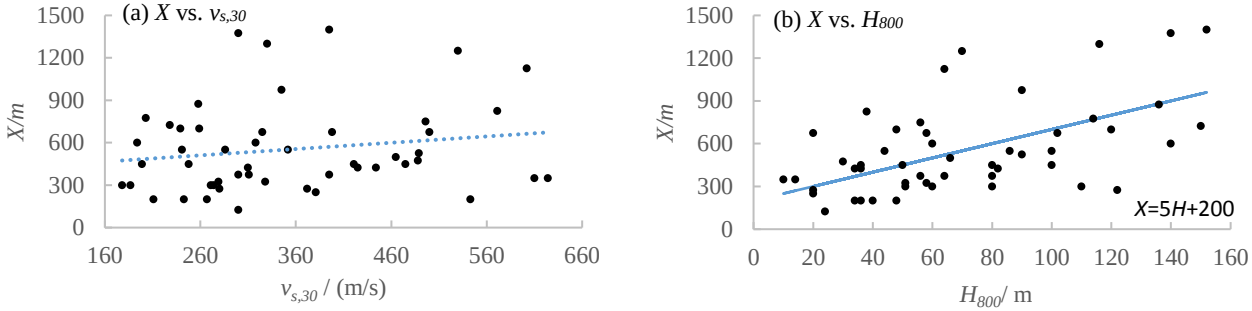


**Fig. 9** Influential area $X$**.** (a) $X$ vs. $v_{s,30}$ ; (b) $X$ vs. $H_{800}$**.**

## 5. Conclusion

With the aim of contributing to quantify the 2D sites of shallow basins, statistics-based numerical study is undertaken in this investigation. Based on the study to a total of 50 vertically heterogeneous shallow basins configured from either real or hypothetic 1D soil profiles, it can be concluded that for a shallow basin, calibration to the acceleration spectra is only needed to locations within the close-to-edge region with a width from the edge $X = 5H_{800} + 200$ by a factor with a maximum around 1.6

## 6. Acknowledgements

This study is sponsored by the China Scholarship Council and the Queensland University of Technology (QUT). The first author would like to acknowledge their supports for this research, and the Pacific Earthquake Engineering Research Center (PEER) for the strong ground motions as well as the KiK-net database for the 1D soil profiles.

## 7. Reference

Aki K, Larner KL (1970) Surface motion of a layered medium having an irregular interface due to incident plane SH waves, J Geophys Res 75: 933-954

Bard PY, Bouchon M (1980a) The seismic response of sediment-filled valleys. Part 1. The case of incident SH waves, Bull Seismol Soc Am 70 (4):1263-1286

Bard PY, Bouchon M (1980b) The seismic response of sediment-filled valleys. Part 2. The case of incident P and SH waves, Bull Seismol Soc Am 70 (5):1921-1941

Bard PY, Bounchon M (1985) The two-dimensional resonance of sediment-filled valleys, Bull Seismol Soc Am 75 (2): 519-541

Campbell, KW (1997) Empirical near-source attenuation relations for horizontal and vertical components of peak ground acceleration, peak ground velocity, and pseudo-absolute acceleration response spectra, Seism. Res. Letters, 68(1):154-179

Chávez-García FJ, Faccioli E (2000) Complex site effects and building codes: making the leap. J Seismol, 4:23–40

Choi Y, Stewart JP (2005) Nonlinear site amplification as function of 30m shear wave velocity, Earthquake Spectra, 21(1), 1-30

Ermert L, Poggi V, Burjanek J, Fah D (2014) Fundamental and higher two-dimensional resonance modes of an Alpine valley. Geophs J Int 198: 795-811

Faccioli E, Vanini M (2003) Complex seismic site effects in sediment-filled valleys and implications on design spectra, Earthquake Engineering and Structural Dynamics, 5(4): 223-238

Field, EH (2000) A modified ground motion attenuation relationship for southern California that accounts for detailed site classification and a basin depth effect, Bull Seism Soc Am, 90, S209-S221
Hanks TC (1975) Strong ground motion of the San Fernando, California, earthquake: Ground displacements, Bull Seism Soc Am 65, 1, 193-225
Hruby CE, Beresnev IA (2003) Empirical corrections for basin effects in stochastic ground motion prediction, based on Los Angeles basin analysis. Bull Seism Soc Am, 93 (4), 1679-1690
Hudson JA (1963) SH Waves in a Wedge-shaped Medium. Geophys J Royal Astr Soc 7 (5): 517-546
King JL, Tucker BE (1984) Observed variations of earthquake motion over a sediment-filled valley, Bull Seism Soc Am 74, 137-152
Lee Y, Anderson JG (2000) A custom southern California ground motion relationship based on analysis of residuals, Bull Seism Soc Am 90, S170-S187
Makra K, Chávez-García FJ (2016) Site effects in 3D basins using 1D and 2D models: an evaluation of the differences based on simulations of the seismic response of Euroseistest. Bulletin of Earthquake Engineering, DOI 10.1007/s10518-015-9862-7
Makra K, Chávez-García FJ, Raptakis D, Pitilaks K (2005) Parametric analysis of the seismic response of a 2D sedimentary valley: Implications for code implementations of complex site effects, Soil Dyn Earthq Eng 19:1-22
Makra K, Gelagoti F, Ktenidou OJ and Pitilakis K (2012) Basin effects in seismic design: efficiency of numerical tools in reproducing complex seismic wavefileds. 15th World Conference on Earthquake Engineering, Lisboa, 2012
Moczo P, Kristek J, Galis M ( 2004) Simulation of planar free surface with near-surface lateral discontinuities in the finite-difference modeling of seismic motion. Bull. Seism. Soc. Am. 94, 760-768
Rail JA and Ling H (1992) Theoretical estimation of the eigenfrequencies of 2-D resonant sedimentary basins: numerical computations and analytical approximations to the elastic problem, Bull Seism Soc Am 82(6):2350-2367
Raptakis D, Makra K, Anastasidis A, Pitilakis (2004) Complex Site Effects in Thessaloniki (Greece): II. 2D SH Modelling and Engineering Insights. Bull Earthq Eng 2: 301-327
Riga E (2015) New elastic spectra, site amplification factors and aggravation factors for complex subsurface geology, towards the improvement of EC8. PhD Thesis dissertation, Aristotle University of Thessaloniki, Greece
Roten D, Fah D, Cornou C, Giardini D (2006) Two-dimensional resonances in Alpine valleys identified from ambient vibration wavefields. Geophs J Int 165: 889-905
Somerville PG, Collins NF, Graves RW, Pitarka A (2004) An engineering ground motion model for basin generated surface waves, Proc. 13th World Conference on Earthquake Engineering, Vancouver, Canada, Paper 515
Trifunac MD (1971) Surface motion of a semi-cylindrical alluvial valley for incident plane SH waves, Bull Seism Soc Am 61:1755-1770
Trifunac MD, Lee VW (1978) Dependence of the Fourier amplitude spectra of strong motion acceleration on the depth of sedimentary deposits, Report No. CE 78-14, University of Southern California, Civil Engineering Department
Tucker BE, King JL (1984) Dependence of sediment-filled valley response on input amplitude and valley properties, Bull Seism Soc Am 74, 153-166
Vessia G, Russo (2013) Relevant features of the valley seismic response: the case study of Tuscan Northern Apennine sector. Bull Earthq Eng 11: 1633-1660
Zhu C, Thambiratnam D (2016). Interaction of geometry and mechanical property of trapezoidal sedimentary basins with incident SH waves, Bull Earthq Eng, DOI 10.1007/s10518-016-9938-z
Zhu C, Thambiratnam D, Zhang J (2015). Response of sedimentary basin to obliquely incident SH waves. Bull Earthq Eng, DOI 10.1007/s10518-015-9856-5
Zhu C, Riga E, Pitilakis K, Zhang J, Thambiratnam D (2016). Geometrical interaction between sedimentary basin and seismic incidence of SV waves. Bull Earthq Eng (under review)

# 8. Appendix

**Table 1** Vertically inhomogeneous basin models configured from 1D soil profiles

| No. | Type | KiK-net Code | $v_{s,30}$ | $H$ ($v_s$=800) | Type | KiK-net Code | $v_{s,30}$ | $H$ ($v_s$ =800) |
|---|---|---|---|---|---|---|---|---|
| 1 | C | AICH16 | 352 | 44 | B | ABSH05 | 624 | 14 |
| 2 | | EHMH09 | 267 | 34 | | ABSH10 | 610 | 10 |
| 3 | | FKIH04 | 300 | 80 | | KGSH01 | 603 | 64 |
| 4 | | FKIH05 | 187 | 80 | | RMIH04 | 543 | 36 |
| 5 | | GIFH06 | 300 | 24 | | KOCH12 | 496 | 56 |
| 6 | | HRSH06 | 279 | 51 | | AKTH01 | 475 | 50 |
| 7 | | HYGH11 | 274 | 51 | | ABSH15 | 465 | 66 |
| 8 | | IBUH07 | 259 | 48 | | ISKH04 | 444 | 82 |
| 9 | | KKWH10 | 328 | 58 | | SMNH03 | 425 | 34 |
| 10 | | KKWH11 | 243 | 48 | | GNMH11 | 421 | 36 |
| 11 | | NGNH32 | 310 | 36 | | YMTH10 | 398 | 102 |
| 12 | | NIGH18 | 311 | 56 | | AICH14 | 395 | 152 |
| 13 | | OSMH01 | 239 | 120 | | NGSH05 | 381 | 20 |
| 14 | | SBSH08 | 325 | 58 | | YMTH07 | 372 | 122 |
| 15 | | SMNH07 | 318 | 60 | | MB1 | 488 | 30 |
| 16 | | SRCH02 | 280 | 20 | | MB2 | 530 | 70 |
| 17 | | YMTH15 | 286 | 86 | | MB3 | 395 | 64 |
| 18 | | MC1 | 345 | 90 | | MB4 | 489 | 90 |
| 19 | | MC2 | 199 | 100 | | MB5 | 500 | 20 |
| 20 | | MC3 | 271 | 110 | | MB6 | 571 | 38 |
| 21 | | MC4 | 248 | 80 | | | | |
| 22 | | MC5 | 300 | 140 | | | | |
| 23 | | MC6 | 178 | 60 | | | | |
| 24 | | MC7 | 211 | 40 | | | | |
| 25 | | MC8 | 241 | 100 | | | | |
| 26 | | MC9 | 194 | 140 | | | | |
| 27 | | MC10 | 228 | 150 | | | | |
| 28 | | MC11 | 330 | 116 | | | | |
| 29 | | MC12 | 258 | 136 | | | | |
| 30 | | MC13 | 203 | 114 | | | | |